Electrochimica Acta, 2021, 390,138816

Electrostatics affects formation of Watson-Crick complex between DNA bases in monolayers of nucleolipids deposited at a gold electrode surface

Francisco Prieto Dapena[a]*, ZhangFei Su[b], Julia Alvarez Malmagro[a,b], Manuela Rueda[a]*, Jacek Lipkowski[b]*

[a] Department of Physical Chemistry, University of Seville, C/Professor García González n◦ 2, 41012 Seville, Spain.

[b] Department of Chemistry, University of Guelph, Guelph, Ontario, Canada N1G 2W1.

Corresponding authors:

Francisco Prieto: dapena@us.es

Manuela Rueda: marueda@us.es

Jacek Lipkowski:jlipkows@uoguelph.ca

In honor of Professor Sergio Trasatti on the occasion of his retirement as editor of Electrochimica Acta and in recognition of his outstanding contributions to electrochemistry

Abstract

Chronocoulometry was applied to determine charge in a monolayer of nucleolipid (1,2-dipalmitoyl-sn-glycero-3-(cytidine diphosphate)) deposited at a gold electrode surface. The immersion method was used to measure the potential of zero charge of the interface (E_{pzci}), which is a sum of charge on the monolayer of the nucleolipid and charge on the gold surface. Photon polarization infrared reflection absorption spectroscopy (PM IRRAS) was used to determine formation of the Watson-Crick complex between terminal cytidine moiety of the nucleolipid and guanine (its complementary base) added to the solution. The combination of electrochemical and spectroscopic studies allowed one to demonstrate that the Watson-Crick complex is formed when the interface is positively charged. The potential applied to the electrode affects not only the complex formation but also orientation of the cytosine moiety. The complex is formed when the cytosine moiety is oriented assuming a small angle with respect to the electrode surface.

1.- Introduction

Lipid monolayers and bilayers supported on solid electrodes constitute systems that mimic, both, the chemical and the electrostatic environments of biological membranes. Therefore, the study of the behavior and the interactions of molecules biologically relevant located on these modified electrodes by electrochemical and spectroelectrochemical methods can provide phenomenological and structural information about their behavior in nature. Additionally, in the case of the DNA bases located on electrode surfaces, their specific Watson-Crick interactions between complementary bases, [1], can be used to develop new electrochemical biosensors.

We have made several efforts to describe molecular recognition reaction between complementary DNA bases at an electrode surface. Our first attempts to study nucleotides directly adsorbed at a gold electrode surface [2–8] were not successful because metal-base interactions were stronger than interactions between co-adsorbed complementary bases. To overcome these limitations, we have employed monolayers of nucleolipids. Nucleolipid monolayers have shown specific molecular recognition capabilities to the complementary DNA bases [9–16]. Therefore, a monolayer of 1,2-dipalmitoyl-sn-glycero-3-(cytidine diphosphate) nucleolipid (16:0 DG-CDP) (Figure 1) was deposited at a gold electrode surface [17]. Since cytidine moiety was separated from the metal surface by a long dipalmitoyl chains, the formation of Watson-Crick with guanine could be observed.[18] The coupling between the C=O stretching vibrations of cytosine and guanine in the Watson-Crick complex was similar to that observed in the complex of polynucleotide helices (poly-cytosine:poly-guanine) [19].

However, the cross section of the polar head group of the nucleolipid is much larger than the cross section of the acyl chains (see Figure 1) and overcrowding of the polar heads could affect the Watson-Crick complex formation. To address this concern a mixed monolayer of DG-CDP and 1,2-dipalmitoyl-sn-glycero-3-phosphocholine (DPPC) was assembled [20]. The DG-CDP and DPPC with (7:3) molar ratio displayed property of an ideal solution in which DG-CDP molecules were diluted by DPPC. Indeed, in the mixed

monolayer the polar head group of the nucleolipid was more parallel to the electrode surface than in the monolayer of pure nucleolipid.

The objective of this work is to explore the molecular recognition capabilities to guanine of mixed monolayers of 16:0 DG-CDP and DPPC transferred to gold electrode surfaces, with higher separation between nucleolipid polar heads than in pure 16:0 DG-CDP monolayers. With the help of chronocoulometry we will determine charge of the polar head of the nucleolipid. We will also determine the potential of zero charge of the interface (E_{pzci}) which corresponds to the sum of charge on monolayer of the nucleolipid and on the surface of the metal, and show that the Watson-Crick complex is formed when the interface is positively charged.

a) 1,2-dipalmitoyl-sn-glycero-3-(cytidine diphosphate) nucelolipid - 16:0 DG-CDP

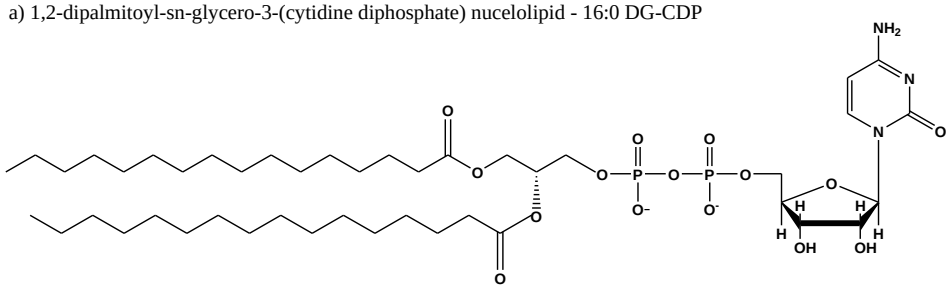

b) 1,2-dipalmitoyl-sn-glycero-3-phosphocholine (DPPC)

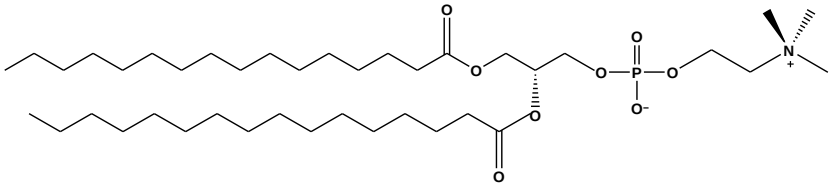

c) Guanine (G)

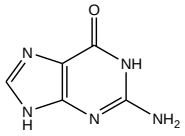

d) Cytosine:Guanine (C:G) complex

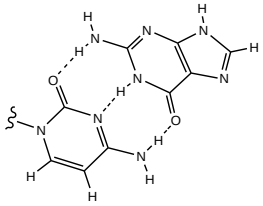

Figure. 1 Molecular structure of a) 1,2-dipalmitoyl-sn-glycero-3-(cytidine diphosphate), b) 1,2-dipalmitoyl-sn-glycero-3-phosphocholine (DPPC) ,c) guanine (G) and d) Cytosine:Guanine (C:G) Watson-Crick complex.

With the help of PM IRRAS we will show that the complex is oriented nearly parallel to the electrode surface. In this way we will provide new information how electrostatics influence the complex formation and orientation of the polar head of the nucleolipid. The data for the mixed monolayer with and without guanine will be compared and the effect of dilution of the nucleolipid with the phospholipid will be discussed.

2.- Experimental.

2.1. Reagents, solutions, and electrodes.

The stock solutions of lipids with the desired mole fraction of 16:0 DG-CDP were prepared by mixing the required volumes of 1 mg mL^{-1} solutions of 1,2-dipalmitoyl-sn-glycero-3-cytidine diphosphate (16:0 CDP DG) and 1,2-dipalmitoyl-sn-glycero-3-phosphocholine (Avanti Polar Lipid) in chloroform. The solutions were stored at -20 °C.

The NaF 0.1 M (Sigma-Aldrich - BioXtra, 99%) supporting electrolyte was prepared from NaF powder cleaned in an UV ozone chamber for 15 min. Ultrapure water, freshly purified with a Milli-Q system was used to make solutions, for electrochemical measurements, and D_2O (Cambridge Isotope Laboratories) was employed to make solutions for PM-IRRAS experiments. The saturated solution of guanine (Sigma-Aldhrich) (c.a. 0.025 mM) was prepered in 0.1 M NaF electrolyte.

The electrochemical and PM-IRRAS measurements were performed in a three-electrode glass cells. Single crystal gold (111) electrodes, home prepared according to the Clavilier method[21], and supplied by Mateck were used as working electrodes for the electrochemical and PM-IRRAS measurements, respectively. Ag/AgCl (saturated KCl, Pine Research Instrumentation, -0.045 V vs SCE) was employed as a reference electrode. The auxiliary electrode was a platinum foil. All the measurements were performed at room temperature (22 ± 2 ℃). All potentials are reported versus the saturated calomel electrode (SCE).

The glassware was cleaned overnight in an acidic solution of potassium permanganate and rinsed first with diluted piranha mixture (3:1 H_2SO_4/H_2O_2 v/v) and next

meticulously rinsed with Milli-Q water. The PTFE components were cleaned by immersion in piranha mixture followed by exhaustive rinsing with Milli-Q water.

2.2. Preparation of the monolayers, measurements of the Langmuir isotherms and transfer of the monolayers to the gold single crystal (111) electrode.

Langmuir isotherms were registered with a Nima 611D Langmuir trough (270 cm^2 of area and c.a. 150 cm^3 of subphase volume), equipped with two PTFE moving barriers and a PS4 pressure sensor and located in a Perspex© cabinet to avoid contamination and air stream interferences. The Wilhelmy plate (a strip of 1 cm-wide Whatman© chromatographic paper) was freshly made for every measurement. The PTFE trough and the moving barriers were cleaned by repetitive rinsing with methanol and Milli Q water.

The mixed monolayers of DPPC and 16:0 DG-CDP were prepared by spreading a volume of 20-30 μL at the air/water interphase in the Langmuir trough with open barriers. The solvent of the lipid solution was allowed to evaporate for 20 min. Then, the barriers compressed the monolayer at a rate of 25 cm^2 min^{1}, while the surface pressure was registered.

The monolayers were transferred to the gold single crystal (111) electrode surfaces at the equilibrium spreading pressure (c.a. 30 mN m^{-1}) by the horizontal touch (Langmuir-Shaefer method) technique. The electrode was previously flame annealed and allowed to cool down in the Langmuir trough cabinet for 30 min. The electrode was horizontally touched to the monolayer using a computer-controlled step motor. It was then immediately lifted. Afterwards, it was dried in Ar atmosphere for 60 min.

2.3. Electrochemical instrumentation and measurements.

Electrochemical measurements were carried out using the HEKA PG590 potentiostat. Before the working electrode was brought into the hanging meniscus configuration, oxygen in the electrolyte solution was removed by purging argon during 30 min. The procedure to measure surface charge densities, was described in the previous paper [17]. The charge density versus potential plots were measured by integrating the current transients registered when potential was stepped from a given potential E to E = -

0.85 V vs SCE [22,23]. The monolayer is completely detached from the gold surface at potential -0.85 V vs SCE. At this potential charge density for the electrode initially covered by the monolayer is equal to charge density at the bare electrode surface. The potential of zero charge for the electrode free from the monolayer was determined independently from the position of the minimum of diffuse double layer on the differential capacity curve. It was used to covert the charge differences between a given potential E and E = -0.85 V vs SCE into the absolute charge densities. The potential of zero free charge of the interface (E_{pzci}) was determined in an independent experiment by the immersion method [24–26]. Figure SI 1 of the supporting information, plots charge densities determined by the immersion method. The intersection of this linear relation with zero charge provided the value of E_{pzci} = 0.08 V vs SCE.

2.4. PM-IRRAS measurements.

Nicolet Nexus 870 (Thermo Fisher) was used to collect PM IRRAS spectra. It was equipped with an external tabletop optical mount (TOM) box which incorporated a MCT-A detector cooled with liquid nitrogen, the sample compartment and the optical head (II/ZS50 ZnSe 50 kHz) of the photoelastic modulator (PEM, PM-90 from Hinds Instruments) and a sampling demodulator (GWC Instruments Synchronous Sampling Demodulator). A CaF_2 equilateral prism (Boxin Photoelectronic Co.) was the IR window as described in [27,28]. The EG&G PAR362 potentiostat was used to control potential of the working electrode. The Omnic software was used for spectra acquisition by means of a macro that triggered the potential steps and the spectra collection.

The gold (111) electrode modified with the nucleolipid monolayer incubated in 0.025 mM guanine solution was transferred to the spectroelectrochemical cell containing 0.1 M NaF in D_2O. The supporting electrolyte was then de-aerated by purging with Ar during 20 min. The electrode was pressed against the rectangular face of the CaF_2 prism, maintaining a thin layer (1-10 μm) of the electrolyte between the electrode and the prism, determined by the procedure described elsewhere [27]. The spectrometer and the TOM box were purged with dry and CO_2 free air from purge gas generator (Parker Blaston). Electrode potential was changed in steps of -0.1 V from 0.36 to -0.85 V vs SCE. At each potential, 4000 interferograms were recorded with an instrument resolution of 4 $cm^{-1}$and averaged.

In order to optimize the mean square electric field strength (MEFS), the incidence of the IR beam and the half-wave retardation of the photoelastic modulator were optimized for different spectral regions (CH stretching region around 3000 cm^{-1} and CO, CC and CN stretching region around 1600 cm^{-1}). The procedure of PM-IRRAS measurements and the signal processing, including the correction of the PEM response functions are described in [27,28].

After correction for PEM response functions, PM-IRRA spectra measure ΔS:

$$\Delta S = \frac{R_p - R_s}{R_p + R_s} = 2.3\ \varepsilon\ \Gamma \qquad (1)$$

where, Rp and R_s are the reflectivities with p and s polarized radiation, Γ is the surface concentration of the absorbing species and ε is the molar absorption coefficient of the adsorbed species. Theoretical PM-IRRA spectra for mixed monolayers of DPPC and 16:0 DG-CDP, with a random orientation of the molecules, were simulated by solving the Fresnel equations for the system of four parallel homogeneous phases (CaF_2|D_2O|DPPC|Au) or (CaF_2|D_2O|16:0 DG-CDP|Au) , as described in [20].

3.- Results and discussion.

3.1. Langmuir isotherms of mixed DG-CDP|DPPC monolayers.

The molecular recognition reaction between guanine and DG-CDP|DPPC monolayer was investigated in 0.1M NaF solution. The compression isotherm of the mixed DG-CDP|DPPC monolayers were studied in [20] using pure water as the subphase. The substitution of water by 0.1M NaF solution was serendipitous. However, it gave very interesting results. Unexpectedly, significant differences between properties of the mixed monolayers spread on 0.1M NaF and on pure water were observed. Figure 2 compares isotherms of DG-CDP|DPPC monolayers measured at the two subphases at different molar fractions of the nucleolipid. The monolayers spread at 0.1M NaF are much more expanded

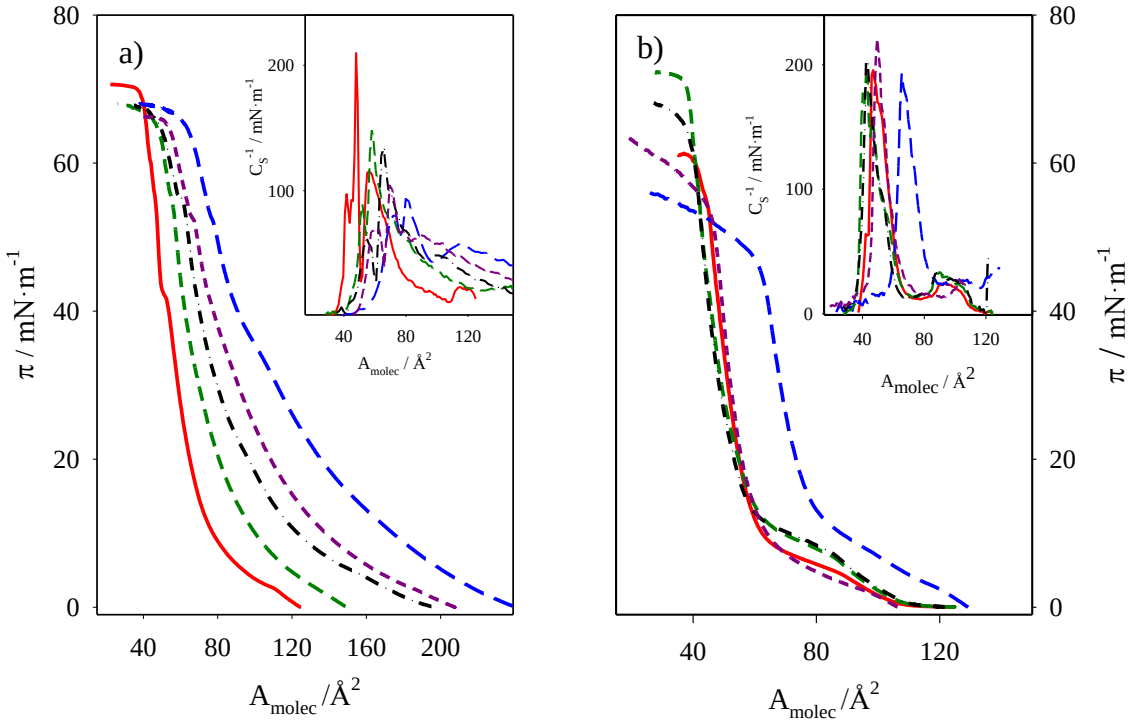

Figure 2. Langmuir isotherms measured at 22°C for the mixed DG-CDP:DPPC monolayers with molar fractions of DG-CDP ($x_{DG\text{-}CDP}$): $x_{DG\text{-}CDP}$ =0 (red solid line), $x_{DG\text{-}CDP}$ =1 (blue dashed line), $x_{DG\text{-}CDP}$ =0.2 (green dashed line), $x_{DG\text{-}CDP}$ =0.4 (black dot-dash line) and $x_{DG\text{-}CDP}$ =0.7 (pink dashed line), measured at aqueous 0.1 M NaF subphase. a), and at pure water subphase, b). Insets plot compression modulus, C_s^{-1}, defined as $C_s^{-1} = -A_{molec}(d\pi/dA_{molec})$ versus the area per molecule. Data for pure water subphase taken from [20].

than that measured at pure H_2O. This is reflected in the onset of compression that takes place at much higher mean molecular areas and in much lower values of the compression modulus than for films compressed at pure water (see insets to Figure 2 a and b). For monolayers spread on 0.1M NaF, the collapse pressure does not change with the mixture composition. In contrast, it changes appreciably for the monolayer spread on H_2O. Such changes are consistent with significant differences in formation of DG-CDP vesicles in pure water and in NaCl solutions observed in [29].

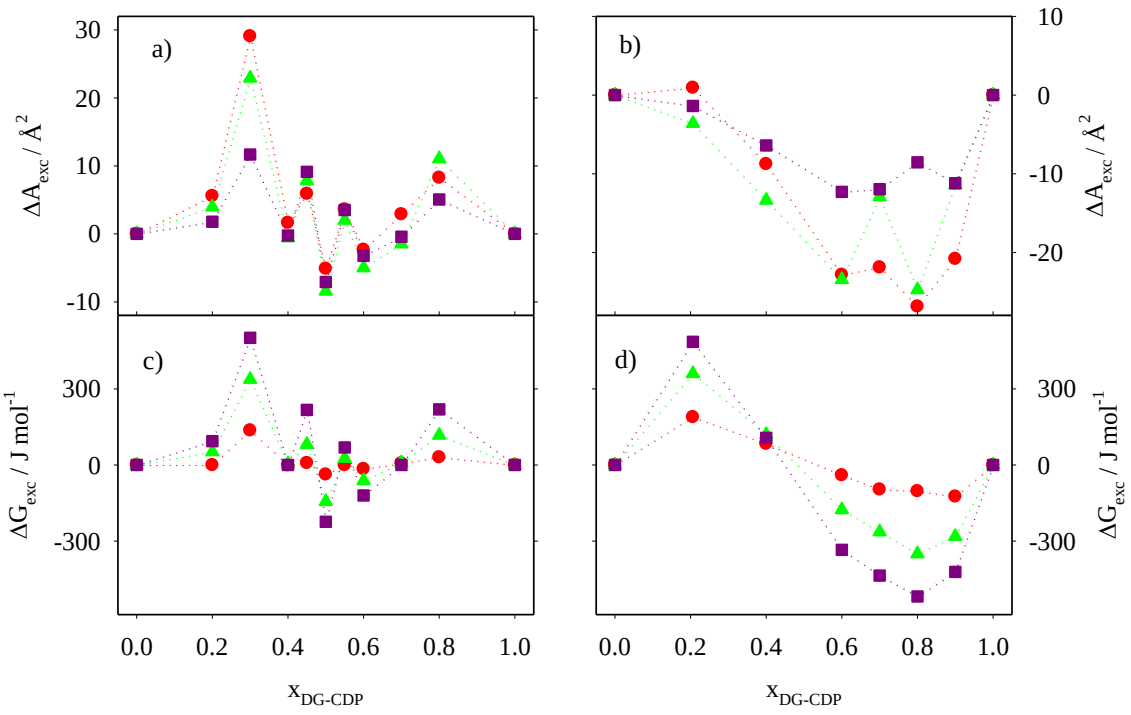

Figure 3. Mean molecular excess area, a) and b), and excess Gibbs free energy, c) and d), plotted as a function of the mole fraction of DG-CDP at surface pressures of 5 mN m^{-1} (red circles), 15 mN m^{-1} (green triangles) and 30 mN m^{-1} (blue squares). Left panel data for 0.1M NaF subphase, right panel data for pure H_2O as the subphase.

The differences between the monolayers spread at H_2O and 0.1M NaF can be quantified by calculating the excess molecular area, ΔA_{exc}:

$$\Delta A_{exc} = A_{molec} - \left(x_{DG-CDP} \cdot A_{(x_{DG-CDP}=0)} + (1 - x_{DG-CDP}) \cdot A_{(x_{DG-CDP}=1)}\right) \qquad (2)$$

and the excess Gibbs energy, ΔG_{exc} defined by:

$$\Delta G_{exc} = \int_0^{\pi} \Delta A_{exc}\, d\pi \qquad (3)$$

They are plotted in Figures 3 a and b. The differences are significant. For monolayers spread at 0.1M NaF both ΔA_{exc} and ΔG_{exc} are predominantly positive, indicating that the interactions between molecules in the monolayer are repulsive. In contrast, for monolayers spread at water both ΔA_{exc} and ΔG_{exc} are negative when the mole fraction of DG-CDP is higher than 0.4, pointing out that the interactions between the molecules in the film are

attractive [20]. The DG-CDP is a dianion. The significant differences between properties of the monolayers spread at the two subphases suggest that the DG-CDP molecules are more ionized in 0.1M NaF solution and their polar heads are more charged in 0.1 M NaF solution than in pure water. The chronocoulometric experiments described in the next section will confirm this conclusion. For the monolayer spread at 0.1M NaF solution at 30 mNm^{-1} both ΔA_{exc} and ΔG_{exc} values are close to zero for the mixture composition 7:3 and the mean molecular área correspond to 90 Å^2.These numbers are characteristic for an ideal solution. Therefore, further experiments will be performed with mixed monolayers of this composition.

3.2. Surface charge density

Figure 4a plots surface charge density vs potential (σ vs *E*) measured at the gold (111) electrode coated with mixed monolayers of DG-CDP:DPPC monolayer (7:3 molar ratio) transferred from 0.1M NaF solution: without guanine (red circles) and incubated in the presence of 0.025 mM guanine (pink squares). For comparison, blue triangles show charge density data of pure DG-CDP monolayer incubated with guanine, taken from ref [18]. The charge density curves show that the mixed monolayer incubated in the presence of guanine is stable at the gold surface in the +0.4 to -0.4 V vs SCE range potentials. The detachment of the monolayer from the electrode surface begins at ~ -0.4V and is completed at E < -0.7 V vs SCE.

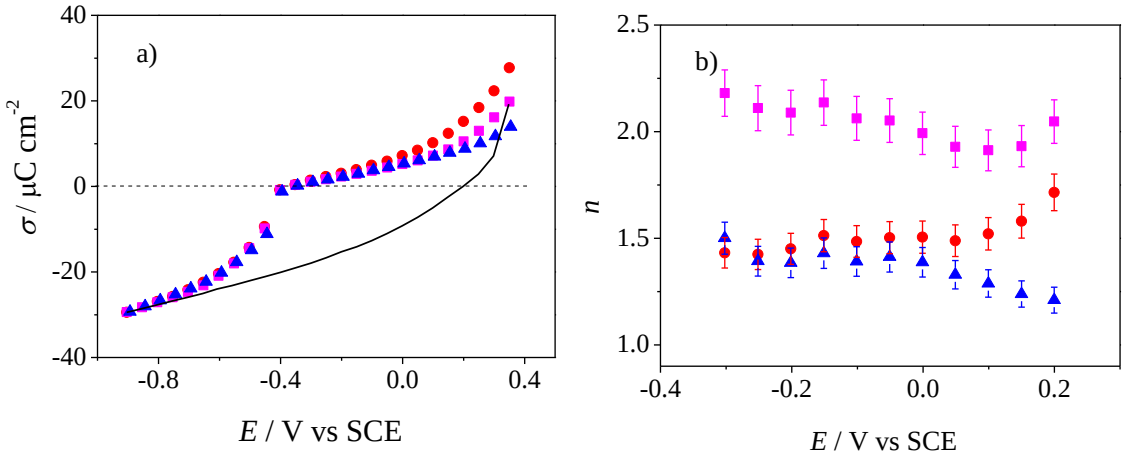

Figure 4 (a). Charge density versus potential curves: **(b)** charge numbers of DG-CDP molecules, for the electrode covered with monolayers transferred from in 0.1M NaF

solution with 0.025 mM guanine (pink squares); the mixed (7:3) DG-CDP:DPPC monolayer without guanine and pure DG-CDP monolayer (blue triangles).

The differences between charge density plots for the three monolayers are small and to a large extent hidden by the differences in the surface concentration of the lipids. To quantify these differences, the electrosorption valencies (*l*) were calculated from the charge density data using the equation:

$$-l = \frac{1}{F}\left(\frac{\sigma_{monolayer} - \sigma_{bare}}{\Gamma}\right)_E \qquad (4)$$

where Γ is the surface concentration of molecules in the monolayer and F is the Faraday constant. In the case of adsorption of charged lipid molecules it has three contributions: i) the work done against charge stored by the monolayer -nFΓ (n is the charge number of DG-CDP molecule) and from charge flowing to the interface due to: (ii) change of the interfacial capacitance and (iii) change of the potential of zero charge. Taking these two contributions into account the electrosorption valency may be expressed by [23,30]:

$$l = \frac{(C_0 - C_1)}{F\,\Gamma}\left(E - E^0_{pzc}\right) - \frac{C_1 E_N}{F\Gamma} - n \qquad (5)$$

where C_0 and C_1 are capacitances of the electrodes that are film free and covered by the monolayer, respectively, E^0_{pzc} is the potential of zero charge of the film free electrode and E_N=(E^1_{pzc}−E^0_{pzc}) is the shift of the potential zero charge due to formation of the monolayer where E^1_{pzc} is the potential of zero total charge of the monolayer covered electrode. The electrosorption valencies calculated from charge density curves are plotted in Figure SI 2 of the Supporting Information. The mean area per molecule equal to 0.90 nm^2 were taken for the film transferred from 0.1 M NaF subphase in the presence of guanine and 0.65 nm^2 for the film transferred from pure water subphase without guanine, at films pressure 30 mNm^{-1}. These numbers were taken from compression isotherms in Figures 2a and 2b. The data for pure CDP-DPPC monolayer were taken from ref [18].

The electrosorption valency data and Equation 5 were then used to calculate the charge numbers n plotted in Figure 4b. The calculations took into account that for mixed films the charge stored by the monolayer is -nF0.7Γ where Γ is the surface concentration calculated from the mean molecular area and 0.7 is the mole fraction of DG-CDP. The charge numbers are equal to ~ 2 for the mixed monolayer with guanine and to ~ 1.5 for the mixed monolayer without guanine and for the monolayer with pure nucleolipid. The DG-CDP is a sodium salt of dianion. The charge number 2 indicates that both phosphate groups of the nucleolipid are dissociated, while the number ~1.5 indicates a partial dissociation of the second phosphate group of the diphosphate moiety of the nucleolipid.

The chronocoulometric experiments measure the total charge, which is charge on the metal plus charge of negatively charged lipids. To evaluate the effect of electrostatic potential that acts on guanine forming complex with the terminal cytidine moiety located at the surface of the monolayer, it is important to determine the potential of zero charge of the interface equal to zero diffuse layer charge. This is the potential at which the charge of the monolayer is fully screened by the opposing charge on the metal (E_{pzci}). This potential can be determined by the immersion method described in [24–26,31].

To determine the E_{pzci}, the DG-CDP:DPPC monolayer was spread on 0.1 M NaF electrolyte surface. The flame-annealed gold (111) electrode was brought in contact with the lipid monolayer at a controlled immersion potential. The transients of current flowing to the interface to form double layer were recorded and integrated to calculate the charge of double layer formation. They are plotted in Figure S1 of the Supporting Information. The linear plot crosses zero charge line at potential at which no diffuse layer is formed. This is the potential of zero charge of the diffuse layer and zero charge of the interface. At this potential, positive charge on the metal is equal to negative charge on the monolayer. The E_{pzci} = 0.08$\pm$0.02 V vs SCE was determined by this method.

3.3. PM-IRRAS measurements

PM-IRRAS spectra have been collected with gold (111) electrodes coated by the mixed monolayer of DG-CDP/DPPC with $x_{DG\text{-}CDP}$=0.7 incubated in the presence of guanine. They were recorded as a function of the electrode potential, in the range of 0.36

to -0.84 V vs SCE. Two different spectral regions have been investigated: 3000-2800 cm^{-1}, at which C-H stretching bands of the acyl chains can be observed, and 1400-1800 cm^{-1}, that includes the C=O stretching bands (at wavenumbers above 1750-1600 cm^{-1}) and the C=N and skeletal vibrations of the cytosine and guanine rings (1450-1600 cm^{-1}).

3.3.1. The 3000-2800 cm^{-1} region (C-H stretching region).

The PM IRRAS spectra in the C-H stretch region of the acyl chains are shown in Figure S4 of the Supporting Information. They are similar to the spectra published in [20] for the monolayer without guanine. The spectra consist of the symmetric and antisymmetric stretching CH_3 and CH_2 vibrations, at c.a. 2850±1 cm^{-1} ($\nu_s(CH_2)$), 2874±1 cm^{-1}($\nu_s(CH_3)$), 2918±1 cm^{-1} ($\nu_{as}(CH_2)$) and 2960±1 cm^{-1} ($\nu_{as}(CH_3)$). The two bands at 2900±1 cm^{-1} and 2938±1 cm^{-1} correspond to the Fermi resonances [27]. The peak positions and the full width at half-maximum (fwhm) of $\nu_s(CH_2)$ (2850±1 cm^{-1} and 10±1 cm^{-1}) and $\nu_{as}(CH_2)$ (2918±1 cm^{-1} and 15±1 cm^{-1}), are similar to the values reported for pure DPPC monolayer in the gel state [32]. They indicate that acyl chains assume predominantly the all-*trans* conformation [33,34].

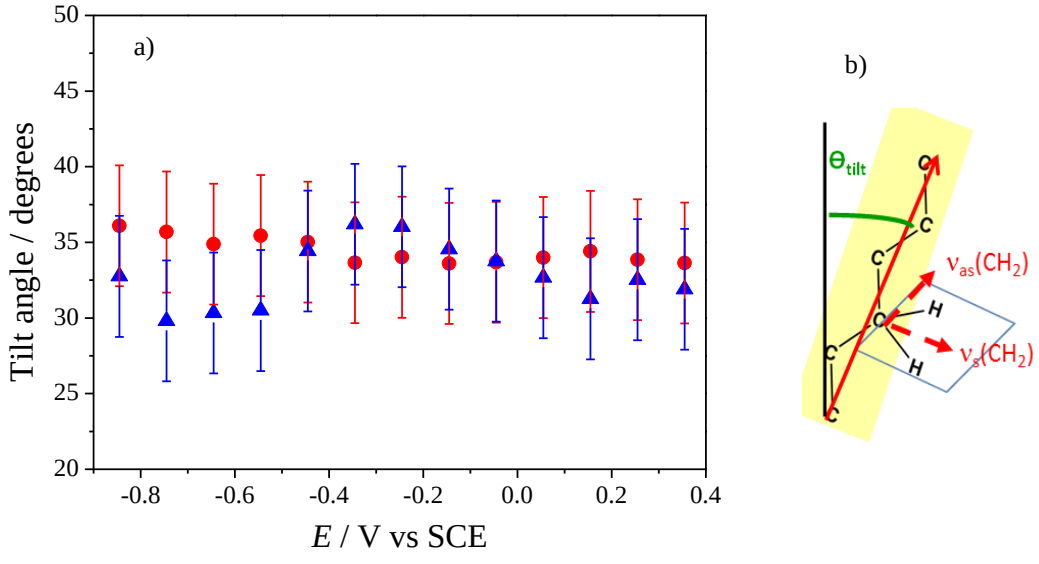

Figure 5. a) Tilt angle vs potential of the acyl chains of mixed DG-CDP:DPPC with x_{DG-CDP}=0.7 incubated in the presence (red circles) and in the absence (blue triangles) of 0.025 mM guanine on gold (111) electrode. b) Scheme of the *all-trans* conformation of the acyl

chain, with the directions of the transition dipoles of $\nu_{s(CH2)}$ and $\nu_{as(CH2),}$ and the tilt angle of the acyl chain, θ_{tilt}.

The integrated intensities of $\nu_{as}(CH_2)$ and $\nu_{s}(CH_2)$ bands could be used to calculate the average tilt angle of trans fragments (θ_{tilt}) of acyl chains. The procedure is described in the Supporting Information. The calculated values of θ_{tilt} are plotted as a function of the electrode potential in Figure 5. For comparison the θ_{tilt} for the mixed monolayer in the absence of guanine are also shown in Figure 5. For the potential range -0.5 to +0.4V vs SCE the tilt angles for the two monolayers are equal within the experimental errors and depend weakly on the electrode potential. Their average value is c.a. 33 degrees. At more negative potentials the monolayers are detached from the electrode surface. However, they remain in the organized state separated from the metal by a thin layer of electrolyte [35,36]. The θ_{tilt} differ somewhat in the detached state, but the changes are small. Overall, the spectra in the C-H stretch region indicate that the presence of guanine has small effect on the packing of the acyl chains.

3.3.2 The polar head region

The polar head spectra can be conveniently divided into two sub-regions, the C=O stretching region 1800-1600 cm^{-1} and the cytosine and guanine ring skeletal vibrations at 1600-1400 cm^{-1}. To reduce the number of figures, the PM-IRRA spectra at different potentials of the polar head region of the mixed DG-CDP/DPPC monolayer incubated in the presence of guanine are shown in Figure S5 of SI. For comparison, the dashed line plots the IR spectrum of the PolyC:PolyG complex in D_2O taken from [19]. Second derivative and two-dimensional correlation spectroscopy (2D-COS) were used to identify the band positions in the spectra. The second derivative of the PM-IRRA spectra obtained at 0.36 V and -0.84 V vs SCE are shown in Figure S6 of SI. To facilitate bands assignment transmission spectra of 5 mM guanosine 5-diphosphate and 5 mM of cytidine 5-diphosphate solutions in D_2O are also included in Figure S6 of SI. The spectra in the two sub-regions will be discussed below separately.

3.3.2.1 The C=O stretching region 1800-1600 cm^{-1}

The IR bands of the Watson-Crick complex and C=O stretch bands of guanine and cytosine are in this region. Figure SI 5 of SI shows that the shape of these spectra change significantly in the 0.36 to -0.24 V vs SCE region.

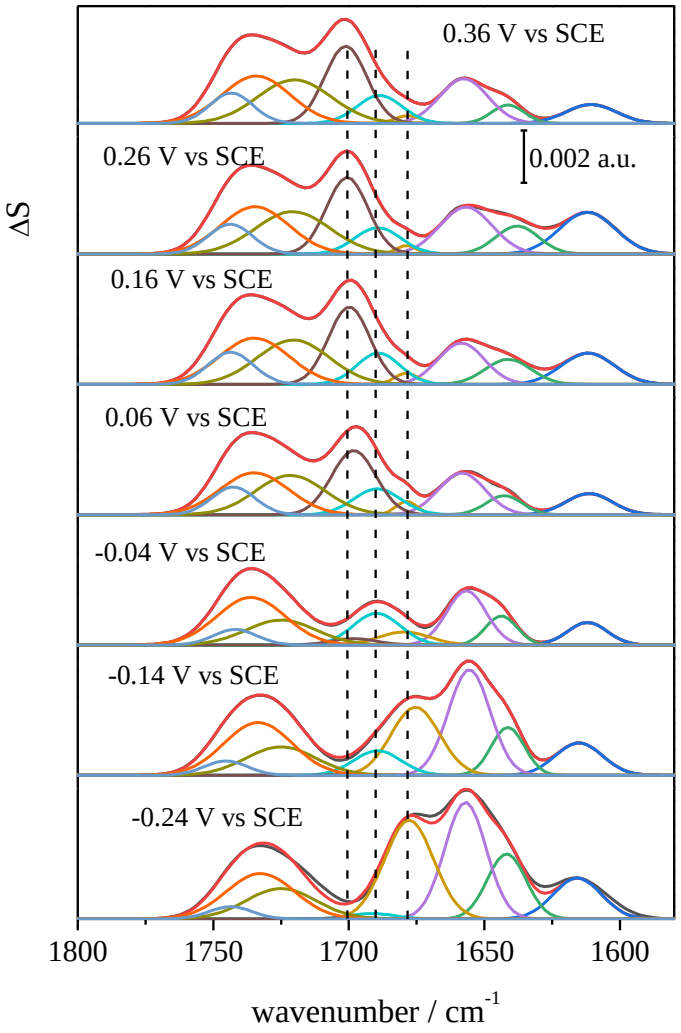

Figure 6. Deconvolution of the PM-IRRA spectra in the potential range 0.36 to -0.24 V vs SCE obtained for a mixed monolayer of DP-CDP:DPPC 7:3 incubated in the presence of 25 μM guanine and transferred to a gold (111) electrode at the equilibrium pressure. Dashed lines are located at 1678, 1690 and 1700 cm^{-1}.

To analyze these changes Figure 6 plots spectra at these potentials. With the help of second derivative and 2D COS the bands were deconvoluted. The three bands at ~1700, 1690 and 1678 cm^{-1} may be assigned to guanine. The band at 1678 cm^{-1} was observed in a

transmission spectrum of guanosine diphosphate and hence may be assigned to non-bonded guanine. The bands at ~1700 and ~1690 cm^{-1} are signatures of Watson-Crick complex and originate from the up-shift of the guanine C=O band caused by intermolecular coupling in the complex [19,37,38]. The presence of two bands suggests presence of complexes with stronger and weaker intermolecular coupling. The bands at 1656, 1645 and 1612 cm^{-1} can be assigned to cytosine moiety The band at 1612 cm^{-1} is assigned to cytosine ring vibrations and bands at 1656, 1645 cm^{-1} are predominantly carbonyl band vibrations coupled to the skeletal C=C vibrations. The coupling gives symmetric and antisymmetric stretches which result in splitting of the cytosine C=O band [37]. Figure SI 7 of SI shows that they are quite sensitive to the molecular environment. Both bands are present in the mixed monolayers. In the presence of guanine, they are somewhat blue shifted. However, in the monolayer of pure nucleolipid with guanine they are significantly blue shifted, and they overlap strongly with the guanine bands. For comparison, in the IR spectrum of dG_5C_5 the double stranded complex shows two carbonyl cytosine bands while the spectrum of $d(GC)_8$ complex has only one carbonyl band. The structure of $d(G_5C_5)$ has A-form and is similar to poly(dG)-poly(dC) while $d(GC)_8$ has B-form structure with alternating G and C bases in the stack. These differences illustrate that the coupling of the carbonyl stretch and C=C stretch vibrations of cytosine is affected by the intermolecular interactions [37].

Consistent with the literature [19,37], the up shift of the C=O guanine band is strong when the Watson-Crick complex is formed and the down shift of the cytosine band is weak. The shape of guanine bands changes significantly with potential while the changes of cytosine bands are less dramatic. This point is illustrated by Figure 7 which plots intensities of guanine and cytosine bands as a function of the electrode potential. The C=O bands of guanine forming complex essentially disappear while the band corresponding to the non-bonded guanine increases at negative potentials.

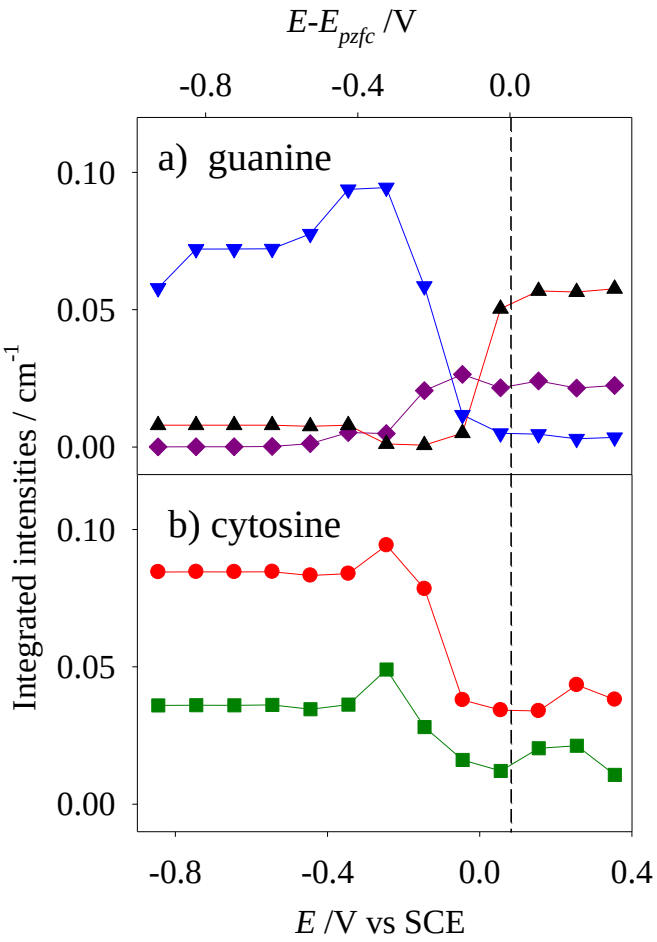

Figure 7. Integrated intensities vs potential plots corresponding to the bands a) at 1678 cm^{-1} (blue triangles-down), 1690 cm^{-1} (purple diamonds) and 1700 cm^{-1} (black triangles-up); b) 1645 (green squares) and 1656 cm^{-1} (red circles), obtained from deconvolution of the PM-IRRA spectra of a mixed monolayer of DP-CDP:DPPC 7:3 incubated in the presence of 25 μM guanine and transferred to a gold (111) electrode at the equilibrium pressure.

This behavior indicates that the complex is stable when the total charge at the interface (charge on the metal plus the charge of the lipid monolayer) is positive, in agreement with the studies of guanine bonding to the monolayer of the pure nucleolipid [18]. In contrast to the behavior of guanine in the complex, the bands of cytosine are increasing by moving from positive to negative potentials. They follow the trend for the band of non-bonded guanine suggesting that complex formation has not strong effect on the cytosine bands. We will show below that the change of the cytosine bands are caused chiefly by the change of the orientation of the cytosine moiety rather than a change of the complex formation/disappearance.

Additional information about the properties of the C=O stretching region is provided by the generalized 2D COS analysis of the spectra. The electrode potential constituted the external perturbation for this analysis (see ref [39]). The 2D COS spectra are shown in Figures 8 a and b in which red color indicates positive bands and blue color negative bands. The synchronous spectra are plotted in Figure 8a. The bands located at the diagonal are auto-correlation bands, the bands located off diagonal are cross-correlation bands. All C=O stretching bands of guanine and cytosine have strong auto-correlation bands. No auto-correlation band is seen for cytosine ring vibrations at ~1612 cm^{-1}. The synchronous spectrum is dominated by strong red square at frequencies between 1675 and 1645 cm^{-1}. It indicates that the non-bonded guanine band at ~ 1678 cm^{-1} and cytosine bands at 1656 and 1645 cm^{-1} are strongly correlated and change in the same direction. The cross-correlation bands of 1675, 1656 and 1645 cm^{-1} with the complexed guanine bands at 1700 and 1690 cm^{-1} indicate that these changes are also correlated but their negative sign indicates that they change in the opposite direction. This result is consistent with plot of intensities in Figure 7.

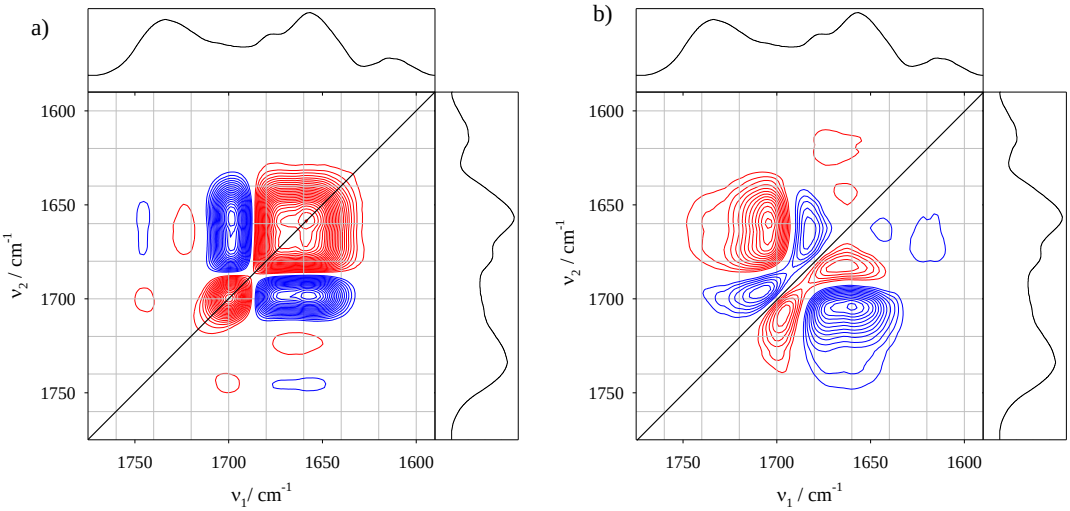

Figure 8. Synchronous ,a) and c), and Asynchronous 2Dcos analysis of the PM-IRRA spectra of the 1800-1600 cm^{-1} , a) and b), and the 1600-1500 cm^{-1}, c) and d), sub-regions of the polar head spectra of a mixed monolayer of DP-CDP:DPPC 7:3 incubated in the

presence of 25 μM guanine and transferred to a gold (111) electrode at the equilibrium pressure. The external variable is the decreasing potential and the reference is the averaged spectrum shown at the axis. Positive cross-correlations are represented in red and negative cross correlations are represented in blue. The diagonals of the surface plots correspond to the autocorrelations.

The asynchronous spectrum Figure 8b provides information about sequential changes of IR bands with potential. It has only cross-correlation bands. The positive sign of the cross-correlation band denoted as (ν_1, ν_2), with ν_1 and ν_2 being wavenumbers on the x and y axes, indicates that changes at ν_1 take place before changes of ν_2. The negative sign indicates that ν_2 precedes ν_1. Table SI 1 of the SI lists signs of the cross-correlation bands. The cross correlation bands at (1645, 1700), (1656, 1700) and (1678, 1700) are negative showing that the potential induced changes of the complex band at 1700 cm^{-1} precedes changes of the non-bonded guanine and cytosine C=O bands. However, the (1690, 1700) band is positive indicating that changes of the "weakly bonded complex" band take place before changes of the "strongly bonded complex" band. Further, (1645, 1678) and (1658, 1678) bands are positive pointing to changes in the cytosine bands are driving the change of the "non bonded" guanine band. The negative sign of the (1645, 1658) band suggests that changes of the 1658 cm^{-1} band precede changes of the 1645 cm^{-1} and that the changes of the two bands are not fully synchronized. Interestingly, the asynchronous spectrum has a negative band at (1612, 1658). The 1612 cm^{-1} ring vibrations band was absent in the synchronous spectrum indicating that its changes are predominantly asynchronous and are to some extent following changes of the main C=O band of cytosine. In conclusion, the 2D COS analysis showed that the potential controlled changes of the spectra are initiated by the changes in the complex followed by the changes of the main cytosine band at 1658 cm^{-1}. The other bands follow the changes of the main cytosine band. Below we will show that this behavior correlates with changes of the orientation of the cytosine moiety with potential.

3.3.2.2 Cytosine and guanine ring vibrations region

For selected potentials between 0.36 and -0.24 V vs SCE, Figure 9 compares deconvoluted spectra in the 1600- 1450 cm^{-1} region, which contains bands corresponding to ring vibrations of cytosine and guanine moiety. The strong bands at 1525 and 1505 cm^{-1} correspond to cytosine moiety and weak bands at 1550, 1567 and 1578 cm^{-1} correspond to guanine. The bands below 1500 cm^{-1} correspond to sugar ring vibrations. The assignment of various bands in the PM IRRAS spectra is summarized in Table SI3 of SI. In addition, Table SI4 lists uncertainties of the band positions, their FWHM and uncertainties of FWHMs.

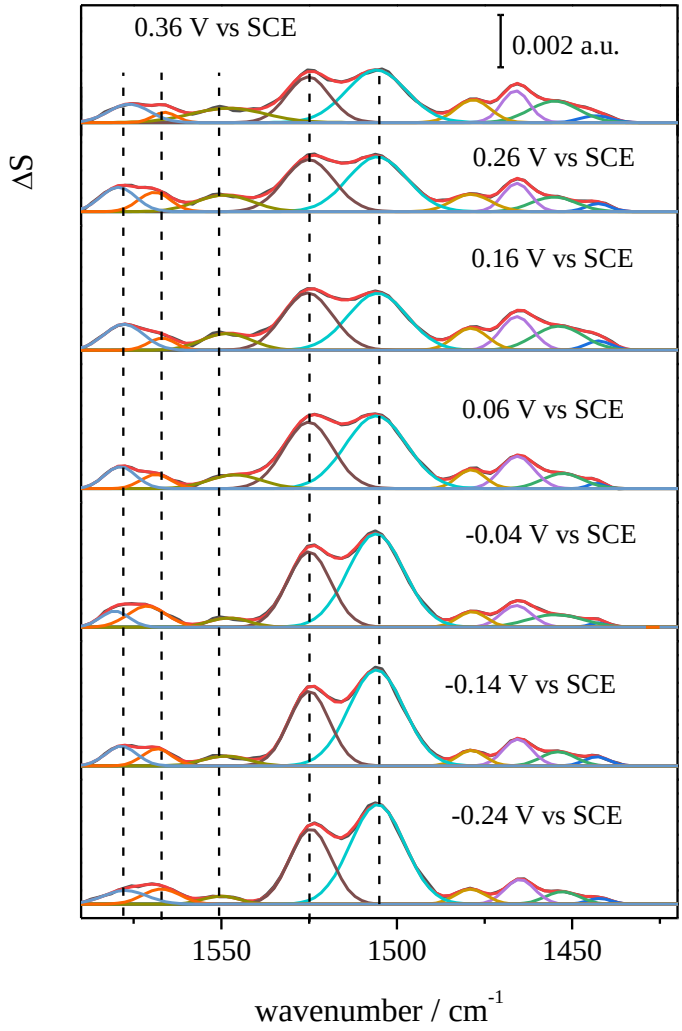

Figure 9. Deconvolution of the PM-IRRA spectra in the potential range 0.36 to -0.24 V vs SCE obtained for a mixed monolayer of DP-CDP:DPPC 7:3 incubated in the presence of 25 μM guanine and transferred to a gold (111) electrode at the equilibrium spreading pressure. Dashed lines are located at 1505, 1525, 1550, 1567 and 1578 cm^{-1}.

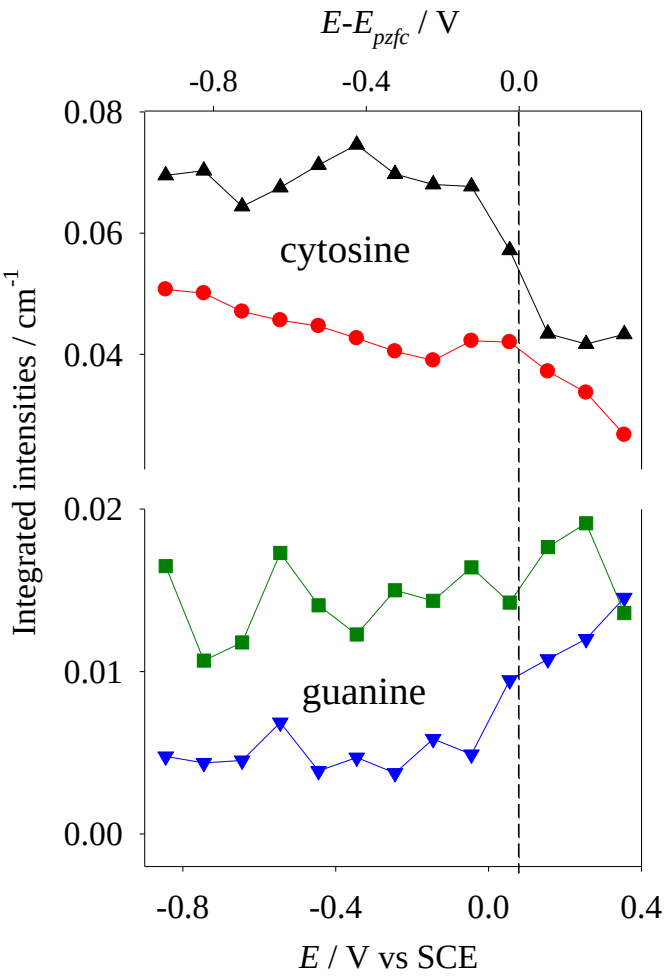

Figure 10. Integrated intensities vs potential plots corresponding to the individual bands at 1505 cm^{-1} (back triangles-up), 1525 cm^{-1} (red circles), 1550 cm^{-1} (blue triangles-down), 1575 cm^{-1} (green squares)), obtained from deconvolution of the PM-IRRA spectra of a mixed monolayer of DP-CDP:DPPC 7:3 incubated in the presence of 25 μM guanine and transferred to a gold (111) electrode at the equilibrium pressure.

Figure 10 plots integrated intensities of cytosine and guanine bands as a function of the electrode potential. The cytosine bands increase while guanine bands decrease when potential becomes more negative. The most dramatic change takes place at the potential of zero charge at the interface. The integrated intensities of the cytosine band can be used to

determine orientation, and rotation of the cytosine moiety as a function of the applied potential using procedure developed in [5,17,18] and described in detail in the Supporting Information.

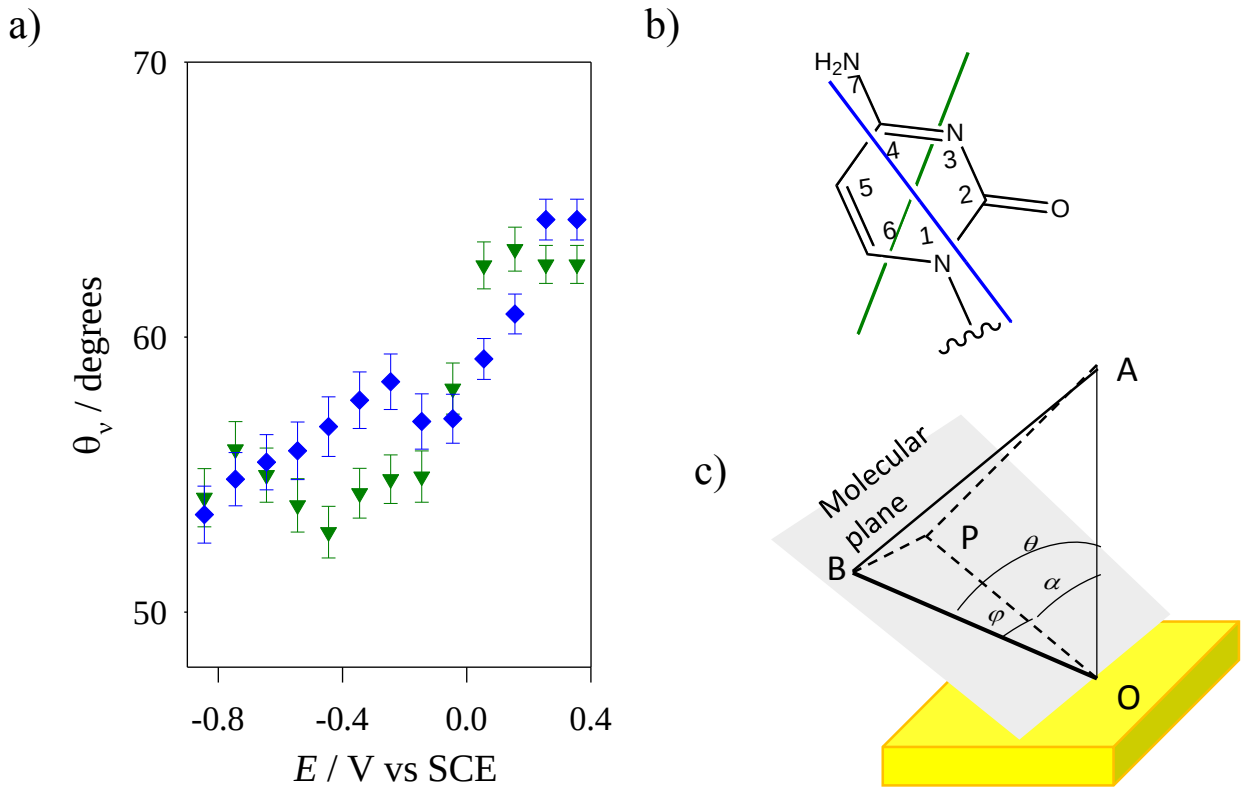

Figure 11. a) Potential dependence of the tilt angles of the vibration tensors of the bands at 1505 (green triangles) and 1525 (blue diamonds) relative to the normal direction to the electrode surface, b) schematic representation of the directions of the transition dipoles of the vibrations at 1505 (green line) and 1525 (blue line) and c) Schematic representation of transition dipole direction of an arbitrary in-plane vibration ($\overline{OB}$), normal direction to the electrode surface ($\overline{OA}$), normal direction to the molecular plane ($\overline{AP}$) and projected normal to the surface onto the molecular plane ($\overline{OP}$).

The integrated intensity is proportional to the $\cos^2\theta$ where θ is the angle between the direction normal to the surface and direction of the transition dipole of a given band. For bands at 1505 and 1525 cm^{-1} the angles θ calculated from the band intensities are plotted in Figure 11a. The directions of the transition dipoles of the 1505 and 1525 cm^{-1} bands of the cytosine moiety were determined with the help of DFT calculations in ref [8].

Their positions are shown in Figure 11b. Since the two transition dipoles are located in plane of the molecule one can calculate angle between surface normal and projection of the surface normal onto the plane of the molecule α and angle φ between direction of the transition dipole and projection of the surface normal onto the molecular plane. The definition of angles θ, α and φ is illustrated by Figure 11c and the procedure employed to calculate these angles is described in the Supporting Information. The angle α is a measure of the tilt of the cytosine moiety with respect to the surface normal while angle φ provides information about its rotation.

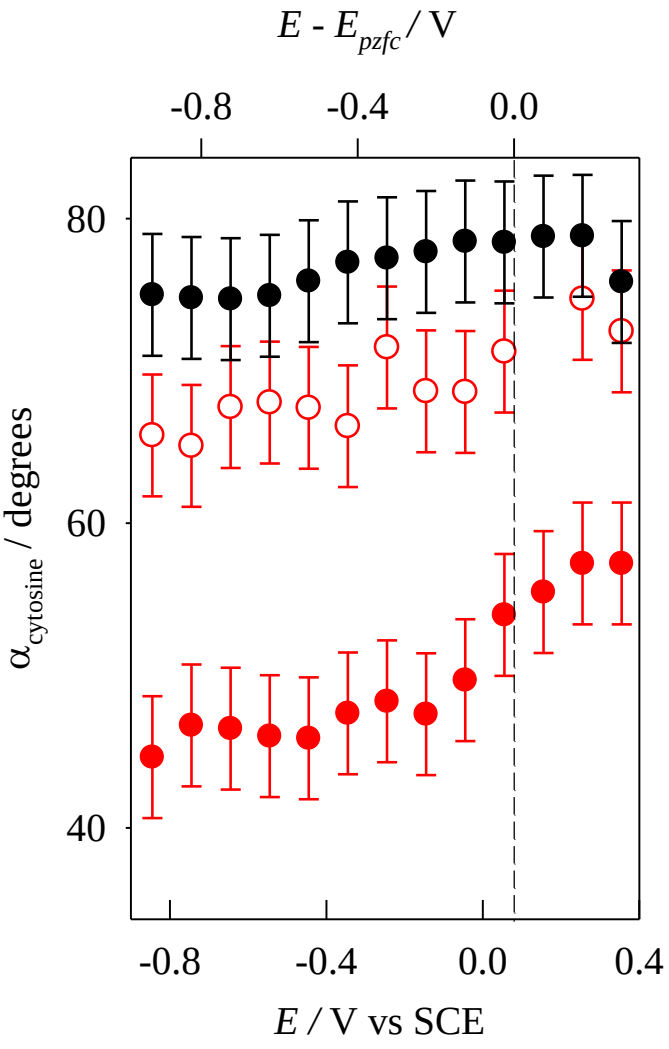

Figure 12. Potential dependence of the tilt angles the cytosine moiety molecular plane for the mixed monolayer of DP-CDP:DPPC 7:3 incubated in the presence of 25 μM guanine and transferred to a gold (111) electrode at the equilibrium pressure (filled red circles) and

in the absence of guanine (hollow red circles) and for a monolayer of pure nucleolipid incubated in the presence of guanine (black filled circles).

Figure 12 compares changes of the tilt of the cytosine plane in the mixed DP-CDP:DPPC 7:3 incubated in the presence of 25 μM guanine, to the orientation in the pure DP-CDP with guanine and in the mixed monolayer without guanine. The plane of cytosine moiety assumes much smaller angle with respect to the normal in the mixed monolayer with guanine than in the mixed monolayer without guanine or pure nucleolipid monolayer with guanine. This trend correlates with the differences between charge of the diphosphate group shown in Figure 4b. The diphosphate group is fully dissociated in the mixed monolayer with guanine and the charge of the polar head group of the nucleolipid is -2, while it is partially dissociated in the two other monolayers where the charge of the diphosphate group is ~ -1.5. The polarity of the head group seems to have influence on the orientation of the cytosine moiety. The orientation of the cytosine moiety also depends on the presence of guanine. It seems that it opens the polar head region assisting in dissociation of the diphosphate group. In the absence of guanine, the cytosine moiety is nearly parallel to the monolayer surface preventing dissociation of the diphosphate group. Smaller tilt of cytosine facilitates sodium transfer into the bulk of the solution. Figure 12 provides second important information. The tilt angle of cytosine moiety is much higher at positive (E-E_{pzfc}) where Watson-Crick complex is stable, indicating that complex assumes a small angle with respect to the plane of the monolayer.

For the 1505 and 1525 cm^{-1} bands, changes of the rotation angles φ with potential are plotted in Figure SI 8a of the Supporting Information. For comparison, Figure SI8 b plots the rotation angles for the mixed monolayer without guanine and Figure SI8 c the rotation angles in pure monolayer of the nucleolipid with guanine. Relative to significant rotations of the plane of cytosine moiety observed in Figures SI 8b and c the rotation in the mixed monolayer with guanine is significantly smaller. Apparently, smaller tilt with respect to the surface normal prevents rotation of the cytosine moiety.

The information concerning sequential changes of the ring stretching bands provides 2D COS analysis shown in Figures SI 9a and b. The synchronous spectra in Figure SI 9a show strong auto-correlation cytosine and weak guanine bands. However, the

guanine bands are present in the cross-correlation peaks that have negative sign indicating that changes of guanine and cytosine bands are in opposite direction. Asynchronous spectra are shown in Figure SI 9b. The (1505, 1525) cross correlation band is negative indicating that changes in 1505 band follow changes of the 1525 band. However, the (1525, 1550) and (1505, 1550) bands are negative suggesting that changes of the guanine band take place earlier than cytosine bands. This trend is consistent with the behavior of C=O stretch bands discussed earlier.

4.Summary and Conclusions

To understand the mechanism of Watson-Crick complex formation between cytidine moiety of a monolayer of nucleolipid DP-CDP and guanine (its complementary base) several experimental techniques and several compositions of the monolayer were employed. The optimal condition for the transfer of the monolayer from the air-solution interface to the gold electrode surface were determined by recording compression isotherms. Monolayers of pure nucleolipid and mixed monolayers of nucleopipid and phospholipids (DPPC) without and with guanine were investigated. Mixed monolayer with composition (7:3) DP-CDP:DPPC molar ratio displayed ideal mixture properties and provided space between polar heads of the nucleolipid. The effect of the static electric field on the properties of the monolayer and the Watson-Crick complex formation was determined by measuring charge density at the electrode surface and the potential of zero charge at the interface. The electrosorption valencies and the charge at the diphosphate group of DP-CDP were calculated. These numbers showed that in the presence of guanine the diphosphate group is totally dissociated while in the monolayer of pure nucleolipid it is partially dissociated. Partial dissociation of the diphosphate group was also observed for the mixed monolayer without guanine. This behavior was explained with the help of PM-IRRAS experiments which showed that cytosine moiety has large tilt angles when the diphosphate group is partially dissociated and smaller tilt angle when it is fully dissociated. The orientation of the cytosine moiety nearly parallel to the monolayer surface constitutes the barrier for exchange of sodium ions between the diphosphate group and the bulk of the solution. In the mixed monolayer with guanine, the guanine molecules promote smaller tilt angle of the cytosine moiety. Since no such effect was observed for a pure monolayer of

DP-CDP one can conclude that more space in the polar head region assists insertion of guanine molecules. Guanine has no effect on the properties of the acyl chains of the lipids suggesting that it is inserted into the polar head region of the monolayers only. IR spectra demonstrated that the monolayers contain two forms of guanine: forming Watson-Crick complex and non-bonded (inserted into the polar head region). The combination of electrochemical and PM IRRAS measurements allowed to show that the Watson-Crick complex is formed only at positively charged interface. Its formation is clearly controlled by electrostatics. When Watson-Crick complex is formed it is oriented assuming small angle with respect to the surface of the monolayer.

The studies described above open the possibility to extend these studies to gold (111) electrodes modified with lipid monolayers incorporating lipid-oligonucleotide conjugates, in order to get recognition to a specific nucleotide sequence. Vesicles containing these compounds have demonstrated their molecular recognition capabilities, by the formation of adducts by Watson-Crick pairing [40]. However, the ratio between hydrophobic chains and negatively charged oligonucleotide fragments will required to be balanced to diminish the electrostatic repulsions [41]. On the other hand, the formation of the Watson-Crick complexes with complementary oligonucleotide will probably modify the dielectric properties of the interface in a magnitude that would facilitate its detection by electrochemical methods.

Acknowledgements

F.P. acknowledges Spain Ministry of Science and Innovation (CTQ2014-57515-C2-1-R and RED2018-102412-T) and Junta de Andaluc á (PAI FQM202). J.L. acknowledges a grant from Natural Sciences and Engineering Research Council of Canada (NSERC) (RG-03958).

References

[1] J.D. Watson, F.H.C. Crick, Molecular Structure of Nucleic Acids: A Structure for Deoxyribose Nucleic Acid, Nature. 171 (1953) 737–738. doi:10.1038/171737a0.

[2] C. Vaz-Dom ínguez, M. Escudero-Escribano, A. Cuesta, F. Prieto-Dapena, C. Cerrillos, M. Rueda, Electrochemical STM study of the adsorption of adenine on

Au(111) electrodes, Electrochem. Commun. 35 (2013) 61–64. doi:10.1016/j.elecom.2013.07.045.

[3] J. Álvarez-Malmagro, F. Prieto, M. Rueda, A. Rodes, In situ Fourier transform infrared reflection absorption spectroscopy study of adenine adsorption on gold electrodes in basic media, Electrochim. Acta. 140 (2014) 476–481. doi:10.1016/j.electacta.2014.03.074.

[4] F. Prieto, J. Alvarez-Malmagro, M. Rueda, J.M. Orts, Tautomerism of adsorbed Thymine on gold electrodes: an in situ surface-enhanced infrared spectroscopy study, Electrochim. Acta. 201 (2016) 300–310. doi:10.1016/j.electacta.2015.11.109.

[5] F. Prieto, Z. Su, J.J.J. Leitch, M. Rueda, J. Lipkowski, Quantitative Subtractively Normalized Interfacial Fourier Transform Infrared Reflection Spectroscopy Study of the Adsorption of Adenine on Au(111) Electrodes, Langmuir. 32 (2016) 3827–3835. doi:10.1021/acs.langmuir.6b00635.

[6] J. Alvarez-Malmagro, M. Rueda, F. Prieto, In situ surface-enhanced infrared spectroscopy study of adenine-thymine co-adsorption on gold electrodes as a function of the pH, J. Electroanal. Chem. 819 (2018) 417–427. doi:/doi.org/10.1016/j.jelechem.2017.11.054.

[7] F. Prieto, M. Rueda, J. Álvarez-Malmagro, Electrochecmical Impedance Spectroscopy analysis of an adsorption process with a coupled preceding chemical step, Electrochim. Acta. 232 (2017) 164–173. doi:10.1016/j.electacta.2017.02.106.

[8] J. Alvarez-Malmagro, F. Prieto, M. Rueda, In Situ Surface Enhanced Infrared Absorption Spectroscopy Study of the Adsorption of Cytosine on Gold Electrodes, J. Electroanal. Chem. 849 (2019) 113362. doi:10.1016/J.JELECHEM.2019.113362.

[9] W. Miao, X. Luo, Y. Liang, Molecular recognition of 7-(2-octadecyloxycarbonylethyl)guanine to cytidine at the air/water interface and LB film studied by Fourier transform infrared spectroscopy, Spectrochim. Acta - Part

A Mol. Biomol. Spectrosc. 59 (2003) 1045–1050. doi:10.1016/S1386-1425(02)00292-5.

[10] W. Miao, X. Du, Y. Liang, Molecular recognition of nucleolipid monolayers of 1-(2-octadecyloxycarbonylethyl)cytosine to guanosine at the air-water interface and Langmuir-Blodgett films, Langmuir. 19 (2003) 5389–5396. doi:10.1021/la0345690.

[11] W. Miao, X. Luo, S. Wu, Y. Liang, Fourier transform infrared spectroscopy study on order-disorder transition in Langmuir-Blodgett films of 7-(2-octadecyloxycarbonylethyl)guanine before and after recognition to cytidine, Spectrochim. Acta - Part A Mol. Biomol. Spectrosc. 60 (2004) 413–416. doi:10.1016/S1386-1425(03)00240-3.

[12] Y. Wang, X. Du, W. Miao, Y. Liang, Molecular recognition of cytosine- and guanine-functionalized nucleolipids in the mixed monolayers at the air-water interface and Langmuir-Blodgett films, J. Phys. Chem. B. 110 (2006) 4914–4923. doi:10.1021/jp055046z.

[13] C. Li, J. Huang, Y. Liang, Molecular Recognition Capabilities of a Nucleolipid Adenosine at the Air / Water Interface and Langmuir-Blodgett Films Studied by Molecular Spectroscopy, Cell. 3 (2000) 7701–7707.

[14] L. Čoga, S. Masiero, I. Drevenšek-Olenik, Lamellar versus compact self-assembly of lipoguanosine derivatives in thin surface films, Colloids Surfaces B Biointerfaces. 121 (2014) 114–121. doi:10.1016/j.colsurfb.2014.05.038.

[15] L. Čoga, L. Spindler, S. Masiero, I. Drevenšek-Olenik, Molecular recognition of a lipophilic guanosine derivative in Langmuir films at the air-water interface, Biochim. Biophys. Acta - Gen. Subj. 1861 (2017) 1463–1470. doi:10.1016/j.bbagen.2016.11.038.

[16] P. G. Argudo, E. Muñoz, J.J. Giner-Casares, M.T. Martín-Romero, L. Camacho, Folding of cytosine-based nucleolipid monolayer by guanine recognition at the air-water interface, J. Colloid Interface Sci. 537 (2019) 694–703.

doi:10.1016/J.JCIS.2018.11.036.

[17] J. Alvarez-Malmagro, Z. Su, J. Jay Leitch, F. Prieto, M. Rueda, J. Lipkowski, Spectroelectrochemical Characterization of 1,2-Dipalmitoyl- sn-glycero-3-cytidine Diphosphate Nucleolipid Monolayer Supported on Gold (111) Electrode, Langmuir. 35 (2019) 901–910. doi:10.1021/acs.langmuir.8b03674.

[18] J. Alvarez-Malmagro, Z. Su, J.J. Leitch, F. Prieto, M. Rueda, J. Lipkowski, Electric-Field-Driven Molecular Recognition Reactions of Guanine with 1,2-Dipalmitoyl- sn - glycero -3-cytidine Monolayers Deposited on Gold Electrodes, Langmuir. 35 (2019) 9297–9307. doi:10.1021/acs.langmuir.9b01238.

[19] F.B. Howarld, J. Frazier, H.T. Miles, Interbase Vibrational Coupling in G: C Polynucleotide Helices, Proc. Natl. Acad. Sci. 64 (1969) 451–458.

[20] F. Prieto-Dapena, Z.F. Su, J. Alvarez-Malmagro, M. Rueda, J. Lipkowski, Mixed monolayer of a nucleolipid and a phospholipid has improved properties for spectroelectrochemical sensing of complementary nucleobasese, J. Electroanal. Chem. in press (2021). doi:https://doi.org/10.1016/j.jelechem.2021.115120.

[21] J. Clavilier, R. Faure, G. Guinet, R. Durand, Preparation of monocrystalline Pt microelectrodes and electrochemical study of the plane surfaces cut in the direction of the {111} and {110} planes, J. Electroanal. Chem. Interfacial Electrochem. 107 (1980) 205–209. doi:10.1016/S0022-0728(79)80022-4.

[22] J. Richer, Measurement of Physical Adsorption of Neutral Organic Species at Solid Electrodes, J. Electrochem. Soc. 133 (1986) 121. doi:10.1149/1.2108505.

[23] J. Kunze, J. Leitch, A.L. Schwan, R.J. Faragher, R. Naumann, S. Schiller, W. Knoll, J.R. Dutcher, J. Lipkowski, New Method to Measure Packing Densities of Self-Assembled Thiolipid Monolayers, (2006). doi:10.1021/la0535274.

[24] Z. Su, J. Leitch, J. Lipkowski, Measurements of the Potentials of Zero Free Charge and Zero Total Charge for 1-thio- ± b β -D-glucose and DPTL Modified Au(111) Surface in Different Electrolyte Solutions, Zeitschrift Für Phys. Chemie. 226

(2012) 995–1009. doi:10.1524/zpch.2012.0280.

[25] P. Ramírez, R. Andreu, Á. Cuesta, C. J. Calzado, J. José Calvente, Determination of the Potential of Zero Charge of Au(111) Modified with Thiol Monolayers, Anal. Chem. 79 (2007) 6473–6479. doi:10.1021/ac071341z.

[26] P. Ramírez, A. Granero, R. Andreu, A. Cuesta, W.H. Mulder, J.J. Calvente, Potential of zero charge as a sensitive probe for the titration of ionizable self-assembled monolayers, Electrochem. Commun. 10 (2008) 1548–1550. doi:10.1016/j.elecom.2008.08.004.

[27] A.H. Kycia, Z. Su, C.L. Brosseau, J. Lipkowski, In Situ PM–IRRAS Studies of Biomimetic Membranes Supported at Gold Electrode Surfaces, in: A. Wieckowski, C. Korzeniewski, B. Braunschweig (Eds.), Vib. Spectrosc. Electrified Interfaces, John Wiley & Sons, 2013: pp. 345–417. doi:10.1002/9781118658871.ch11.

[28] V. Zamlynny, J. Lipkowski, Quantitative SNIFTIRS and PM IRRAS of Organic Molecules at Electrode Surfaces, in: R.C. Alkire, D.M. Kolb, J. Lipkowski, P. Ross (Eds.), Adv. Electrochem. Sci. Eng., Wiley-VCH Verlag GmbH, 2006: pp. 315–376. doi:10.1002/9783527616817.ch9.

[29] B. Alies, M.A. Ouelhazi, A. Patwa, J. Verget, L. Navailles, V. Desvergnes, P. Barthélémy, Cytidine-and guanosine-based nucleotide-lipids, 2018. http://www.rsc.org/suppdata/c8/ob/c8ob01023d/c8ob01023d1.pdf (accessed December 25, 2018).

[30] T. Laredo, J. Leitch, M. Chen, I. J. Burgess, J. R. Dutcher, J. Lipkowski, Measurement of the Charge Number Per Adsorbed Molecule and Packing Densities of Self-Assembled Long-Chain Monolayers of Thiols, Langmuir. 23 (2007) 6205–6211. doi:10.1021/la070202+.

[31] U.W. Hamm, D. Kramer, R.S. Zhai, D.M. Kolb, The pzc of Au(111) and Pt(111) in a perchloric acid solution: An ex situ approach to the immersion technique, J. Electroanal. Chem. 414 (1996) 85–89. doi:10.1016/0022-0728(96)01006-6.

[32] R. A. Dluhy, R. Mendelsohn, H. L. Casal, H. H. Mantsch, Interaction of dipalmitoylphosphatidylcholine and dimyristoylphosphatidylcholine-d54 mixtures with glycophorin. A Fourier transform infrared investigation, Biochemistry. 22 (2002) 1170–1177. doi:10.1021/bi00274a028.

[33] H.L. Casal, H. Mantsch, Polymorphic phase behaviour of phospholipid membranes studied by infrared spectroscopy, Biochim. Biophys. Acta - Biomembr. 779 (1984) 381–401.

[34] H.H. Mantsch, R.N. McElhaney, Phospholipid phase transitions in model and biological membranes as studied by infrared spectroscopy, Chem. Phys. Lipids. 57 (1991) 213–226. doi:10.1016/0009-3084(91)90077-O.

[35] I. Burgess, M. Li, S.L. Horswell, G. Szymanski, J. Lipkowski, J. Majewski, S. Satija, Electric Field-Driven Transformations of a Supported Model Biological Membrane - An Electrochemical and Neutron Reflectivity Study, Biophys. J. 86 (2004) 1763–1776. doi:10.1016/S0006-3495(04)74244-7.

[36] I. Zawisza, I. Burgess, G. Szymanski, J. Lipkowski, J. Majewski, S. Satija, Electrochemical, neutron reflectivity and in situ PM-FT-IRRAS studies of a monolayer of n-octadecanol at a Au(1 1 1) electrode surface, in: Electrochim. Acta, Pergamon, 2004: pp. 3651–3664. doi:10.1016/j.electacta.2004.02.051.

[37] A.T. Krummel, M.T. Zanni, DNA Vibrational Coupling Revealed with Two-Dimensional Infrared Spectroscopy: Insight into Why Vibrational Spectroscopy Is Sensitive to DNA Structure, J. Phys. Chem. B. 110 (2006) 13991–14000. doi:10.1021/jp062597w.

[38] C. Lee, K.-H.H. Park, M. Cho, Vibrational dynamics of DNA. I. Vibrational basis modes and couplings, J. Chem. Phys. 125 (2006) 114508. doi:10.1063/1.2213257.

[39] I. Noda, Generalized Two-Dimensional Correlation Method Applicable to Infrared, Raman, and other Types of Spectroscopy, Appl. Spectrosc. 47 (1993) 1329–1336. doi:10.1366/0003702934067694.

[40] X. Li, K. Feng, L. Li, L. Yang, X. Pan, H.S. Yazd, C. Cui, J. Li, L. Moroz, Y. Sun, B. Wang, X. Li, T. Huang, W. Tan, Lipid-oligonucleotide conjugates for bioapplications, Natl. Sci. Rev. 7 (2020) 1933–1953. doi:10.1093/nsr/nwaa161.

[41] M. P. Thompson, M.-P. Chien, T.-H. Ku, A. M. Rush, N. C. Gianneschi, Smart Lipids for Programmable Nanomaterials, Nano Lett. 10 (2010) 2690–2693. doi:10.1021/nl101640k.